ACS APPLIED MATERIALS & INTERFACES

www.acsami.org

Research Article

Investigating the Influence of Metal–Organic Framework Loading on the Filtration Performance of Electrospun Nanofiber Air Filters

Zhuolun Niu, Can Xiao, Jinhan Mo, Li Zhang, and Chun Chen*

Cite This: *ACS Appl. Mater. Interfaces* 2022, 14, 27096–27106

Read Online

ACCESS | Metrics & More | Article Recommendations

ABSTRACT: Integrating metal–organic frameworks (MOFs) into electrospun nanofiber filters has become an effective method for improving particle filtration efficiency. This study hypothesized that there is an optimal amount of MOFs that can be integrated into electrospun nanofiber filters to achieve the maximum particle removal efficiency while minimizing the corresponding MOF synthesis time. To test the hypothesis, this study systematically explored the influence of the time-dependent in situ growing process of zeolitic imidazolate framework-67 (ZIF-67), a typical type of MOFs, on the filtration performance of polyacrylonitrile (PAN) electrospun nanofibers. The results show that the surface morphology and chemical composition of the PAN/ZIF-67 hybrid nanofiber filters gradually changed with the reaction time. For PAN/ZIF-67 hybrid nanofiber filters with relatively low initial $PM_{0.3-0.4}$ filtration efficiency, a reaction time of only 5 min was sufficient for the synthesis of the amount of ZIF-67 that maximized the $PM_{0.3-0.4}$ filtration efficiency. However, for thick filters with high original $PM_{0.3-0.4}$ filtration efficiency (>90%), the integration of ZIF-67 was not necessary, because the efficiency enhancement would not be significant. In addition, the enhancement of filtration efficiency for ultrafine particles was positively correlated with the amount of incorporated ZIF-67. In summary, this study shortened the synthesis time of the in situ incorporation of MOFs into electrospun nanofiber filters from more than 10 h (reported in the literature) to only 5 min.

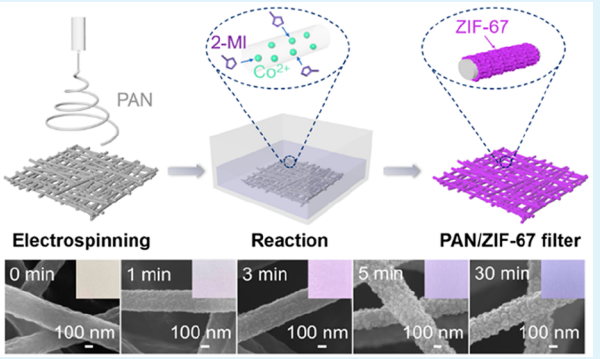

KEYWORDS: *indoor air quality, metal–organic frameworks, particulate matter, electrospinning, filtration efficiency*

1. INTRODUCTION

In recent decades, air pollution in both indoor and outdoor environments has aroused increasing research interest because of its adverse effects on human health. According to the World Health Organization (WHO), human deaths as a result of exposure to ambient air pollution amount to around 4.2 million every year.[1] Among the air pollutants, particulate matter (PM), is one of the major public health concerns, and it can be classified by aerodynamic diameter (d_p): coarse (d_p > 2.5 μm), fine (d_p = 0.1–2.5 μm), and ultrafine particles (UPFs, d_p < 0.1 μm or 100 nm).[2] Fine particles ($PM_{2.5}$) are a leading threat to morbidity and mortality.[3−5] UPFs with smaller sizes and larger surface areas have been proved to cause inflammatory and cardiovascular changes,[6] and even to be travel through the olfactory neuronal pathway and affect the central nervous system.[7] Furthermore, according to an aerodynamic analysis in two Wuhan hospitals, severe acute respiratory syndrome coronavirus 2 (SARS-CoV-2), which is the virus that caused the coronavirus disease 2019 (COVID-19) pandemic, can adhere to aerosols and be transferred in the air.[8] Therefore, it is crucial to reduce particle concentrations in both indoor and outdoor environments for protecting public health.

Filtration is among the most effective measures for reducing the number of airborne particles. According to classical theory, the particle filtration mechanisms of fibrous filters include inertial impaction, interception, Brownian diffusion, gravitational settling, and electrostatic effect.[9−11] Therefore, cost-effective fibrous filters have been widely used in heating, ventilation, and air-conditioning (HVAC) systems for air filtration.[12−14] However, traditional high-efficiency particulate air (HEPA) filters are composed of many layers of microfibers and exhibit a high pressure drop with increased energy consumption.[15,16] As nanotechnology has developed, electrospinning has become a fascinating technique for fabricating nanofiber air filters with high particle removal efficiency,

Received: April 18, 2022
Accepted: May 20, 2022
Published: June 3, 2022

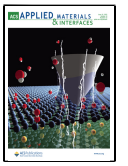

https://doi.org/10.1021/acsami.2c06808
ACS Appl. Mater. Interfaces 2022, 14, 27096–27106

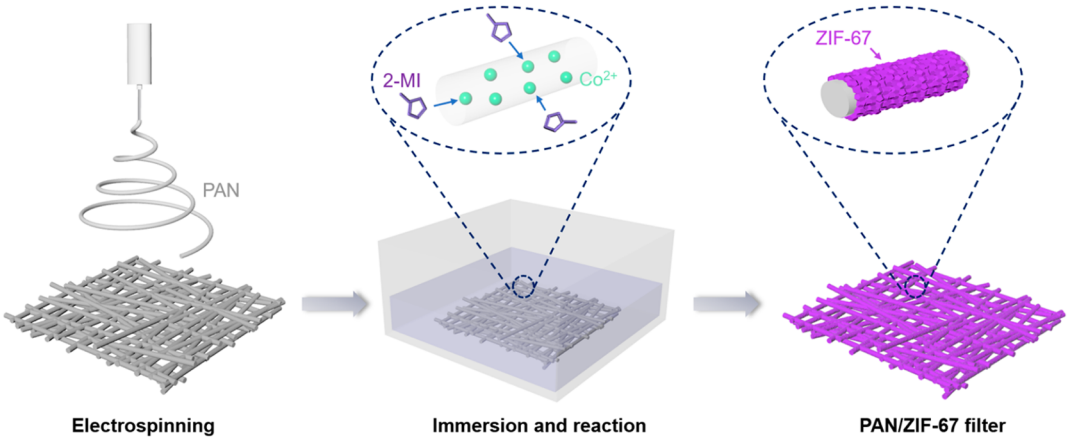

Figure 1. Schematic illustration of fabrication of electrospun nanofiber filters and in situ growth of ZIF-67.

flexible morphology, and excellent chemical and physical properties.[17,18] Because of the nanoscale diameter of electrospun fibers, the slip-flow effect can emerge, which leads to lower drag force and pressure drop.[19] Therefore, electrospun nanofiber filters have shown excellent application potential in the area of particle filtration.[20,21] Moreover, through surface modification or the introduction of additives, electrospun nanofiber filters can be further adjusted to achieve tunable and versatile filtration properties.[22−26]

Metal−organic frameworks (MOFs) are composed of metal ions and organic ligands, and they play a vital role in energy and environmental applications.[27−29] Recently, fiber-based composites combining MOFs and polymers by means of MOF-first,[30] fiber-first,[31] and MOF attachment[32] strategies have seen tremendous development.[23] Some of the particulate matter in the air exhibits high polarity because chemical groups such as C−O, C═O, and C−N are present on the outer surface.[33−35] The large numbers of open metal sites and unbalanced ions of MOFs help to attract these high-polarity particles electrostatically.[33,36] Zhang et al. used an MOF-first strategy to fabricate various kinds of MOF-based filters, which exhibited high filtration efficiency for PM generated by burning incense ($PM_{2.5}$ 88.33 ± 1.52% and PM_{10} 89.67 ± 1.33%).[30] Bian et al. developed an immersion method to embed MOFs into PAN electrospun nanofiber filters, achieving high removal efficiency for both formaldehyde (84%) and incense $PM_{2.5}$ (99%).[37] Liang et al. created self-supported MOF fibrous mats by combining electrospinning and a phase transformation reaction; these mats exhibited an excellent removal efficiency of 89% for $PM_{2.5}$.[38] These studies have demonstrated that MOF-based nanofiber air filters can achieve remarkable particle filtration efficiency. However, the fabrication of these filters has involved a time-consuming synthesis procedure, which may not be sufficiently practical in large-scale production. For example, in the MOF-first strategy for nanofiber filters, the preparation time for MOF crystals ranged from 24 h (e.g., for ZIF-8) to 4 days (e.g., for Mg-MOF-74).[30] Fabricating MOF-based nanofiber air filters by an in situ growth process was much simpler than the MOF-first strategy; however, it still took 10−24 h (e.g., for ZIF-67) to incorporate MOFs into electrospun filters.[37,39] Therefore, it would be worthwhile to improve the fabrication methods to shorten the procedure for MOF synthesis on electrospun nanofiber filters.

To the best of our knowledge, few studies, if any, have attempted to shorten the procedure for MOF synthesis on electrospun nanofiber filters by investigating the influence of MOF loading on particle filtration efficiency. Theoretically, the integration of larger amounts of MOFs into electrospun nanofiber filters would increase the particle removal efficiency because of electrostatic effects and increased roughness. However, when the nanofibers are already fully covered by MOFs, a longer reaction time will not increase the amount of integrated MOFs and thus the particle filtration efficiency. This study hypothesized that there is an optimal amount of MOFs that can be integrated into electrospun nanofiber filters to achieve the maximum particle removal efficiency while minimizing the corresponding MOF synthesis time. To test the hypothesis, this study systematically investigated the time-dependent in situ growth of zeolitic imidazolate framework-67 (ZIF-67), a typical MOF formed by bridging 2-methylimidazolate and Co^{2+} ions,[40,41] on the surface of electrospun PAN nanofiber filters. The relationship between the amount of ZIF-67 integrated into the filters and the size-dependent particle filtration efficiency was explored under different face velocities and filter thicknesses. The optimal amounts of the MOF and the corresponding synthesis times were obtained for the fabricated PAN/ZIF-67 hybrid nanofiber filters.

2. METHODS

2.1. Electrospinning of Precursor Nanofibers. First, a 6 wt % polyacrylonitrile (PAN, M_w = 150 000 g/mol, Sigma-Aldrich, USA) polymer solution was prepared by dissolving 0.5 g of PAN into 7.83 g of dimethylformamide (DMF, RCI Labscan, Thailand) and magnetically stirring for 2 h at room temperature. Next, 0.5 g cobalt acetate tetrahydrate ($Co(Ac)_2{\cdot}4H_2O$, AR, 99.5%, Aladdin, China) was added to the PAN polymer solution, which was stirred for another hour to form a homogeneous solution. The prepared PAN/$Co(Ac)_2$ solution was poured into a 10 mL syringe connected to a metallic needle (22 gauge). A high DC voltage of 15 kV was applied between the needle tip and a grounded roller, which was covered with a copper mesh as a substrate. During the electrospinning process, the solution injection rate was set at 1.5 mL/h, and the tip-to-roller distance was set at 20 cm. There groups of filters with different thicknesses were fabricated by adjusting the electrospinning time (t_s) to 1, 1.5, and 3 h, respectively. To ensure the stability of the electrospinning process, we controlled the temperature and relative humidity at 23 ± 2 °C and 50 ± 3%, respectively.

2.2. In Situ Growth of ZIF-67 Crystals on PAN Nanofibers. One gram of 2-methylimidazole (2-MI, 98%, Aladdin, China) was dissolved in 100 mL of ethanol (GC, 99.99%, Daejung, Korea) to prepare the 2-MI/ethanol precursor solution. Next, the as-spun filters (10 × 10 cm^2) were immersed in the 2-MI/ethanol for the in situ

https://doi.org/10.1021/acsami.2c06808
ACS Appl. Mater. Interfaces 2022, 14, 27096−27106

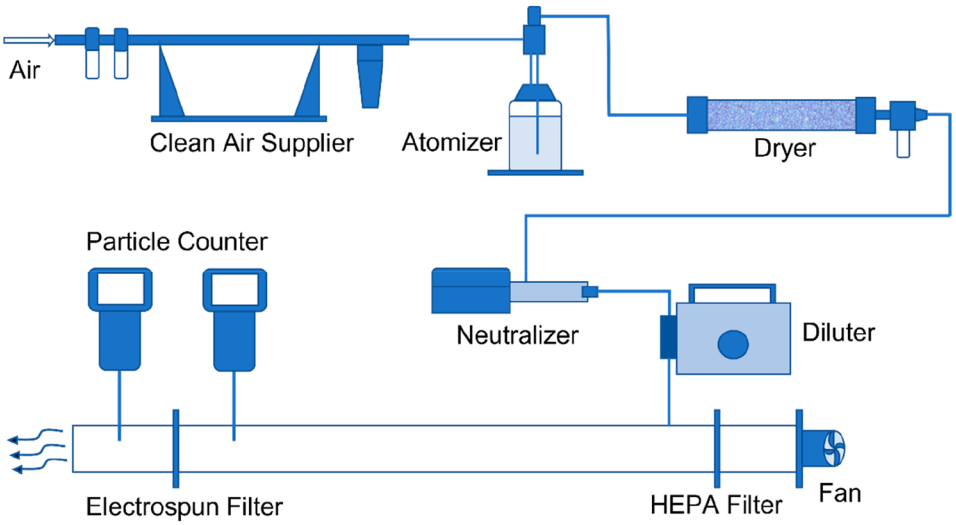

Figure 2. Experimental setup for testing the filtration performance.

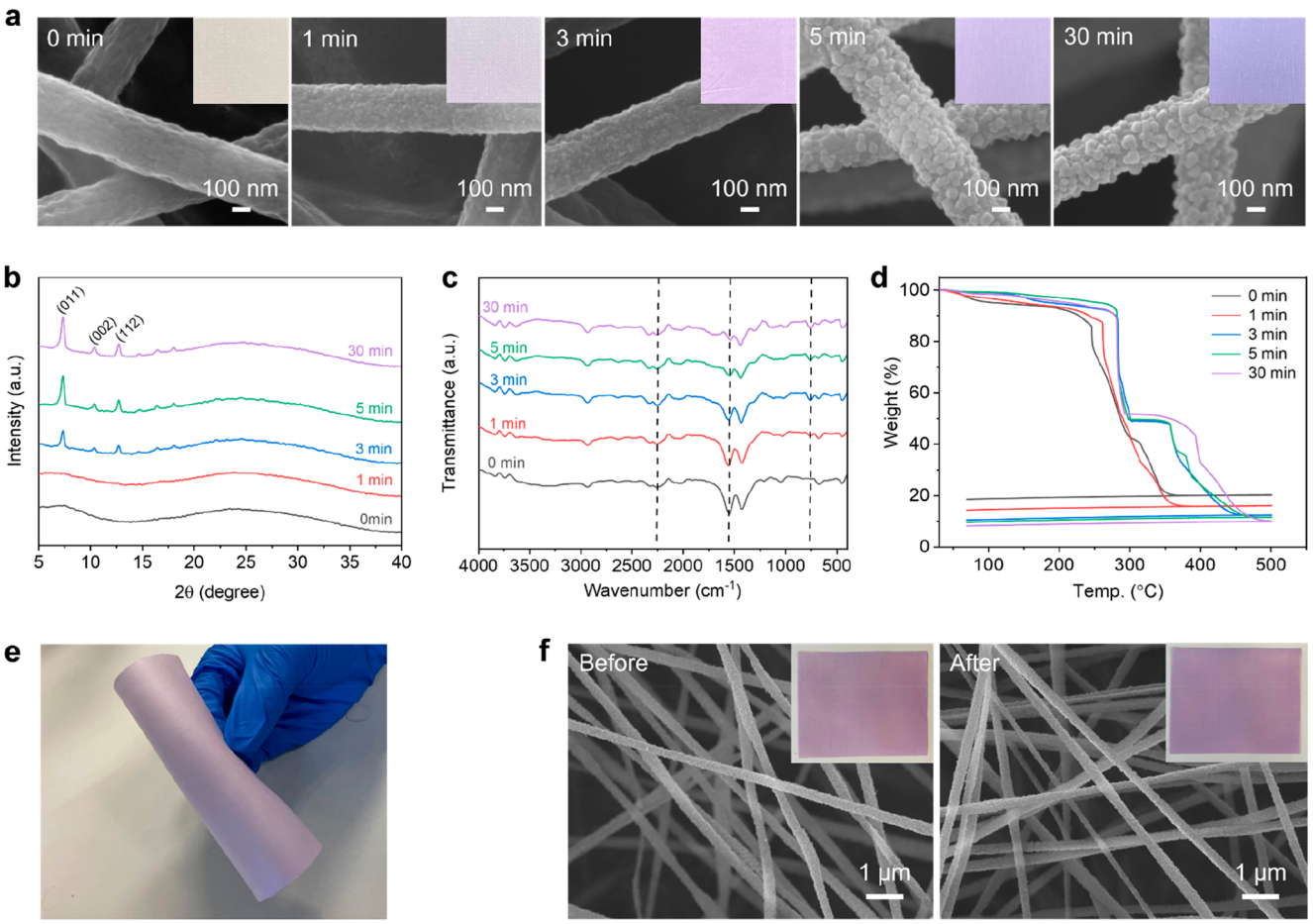

Figure 3. Characterizations of PAN/ZIF-67 hybrid nanofiber filters with different reaction times: (a) SEM and photographic images, (b) XRD patterns, (c) FTIR spectroscopy, (d) TGA curve, (e) photographic image of a bent PAN/ZIF-67 hybrid nanofiber filter, and (f) SEM and photographic images of a PAN/ZIF-67 hybrid nanofiber filter before and after being used under a strong wind (10 m/s) for 1 h.

growth of ZIF-67. During the reaction, the cobalt ions in the nanofibers coordinated with the 2-MI in the solution, and the ZIF-67 crystals were in situ synthesized on the surface of the PAN nanofibers (as shown in Figure 1). The reaction time was controlled at 1, 3, 5, and 30 min to fabricate filters with different ZIF-67 loading levels. In addition, another group of filters without reaction was set as a control group (i.e., reacted for 0 min). After the immersion process, the filters were washed in ethanol several times to completely remove the residue precursor solution. Finally, the filters were dried in an electric drying oven (DHG-9075A, Shanghai Yiheng, China) for 10 min. The fabricated PAN/ZIF-67 hybrid nanofiber filters could then serve as air filters for capturing particles.

https://doi.org/10.1021/acsami.2c06808
ACS Appl. Mater. Interfaces 2022, 14, 27096−27106

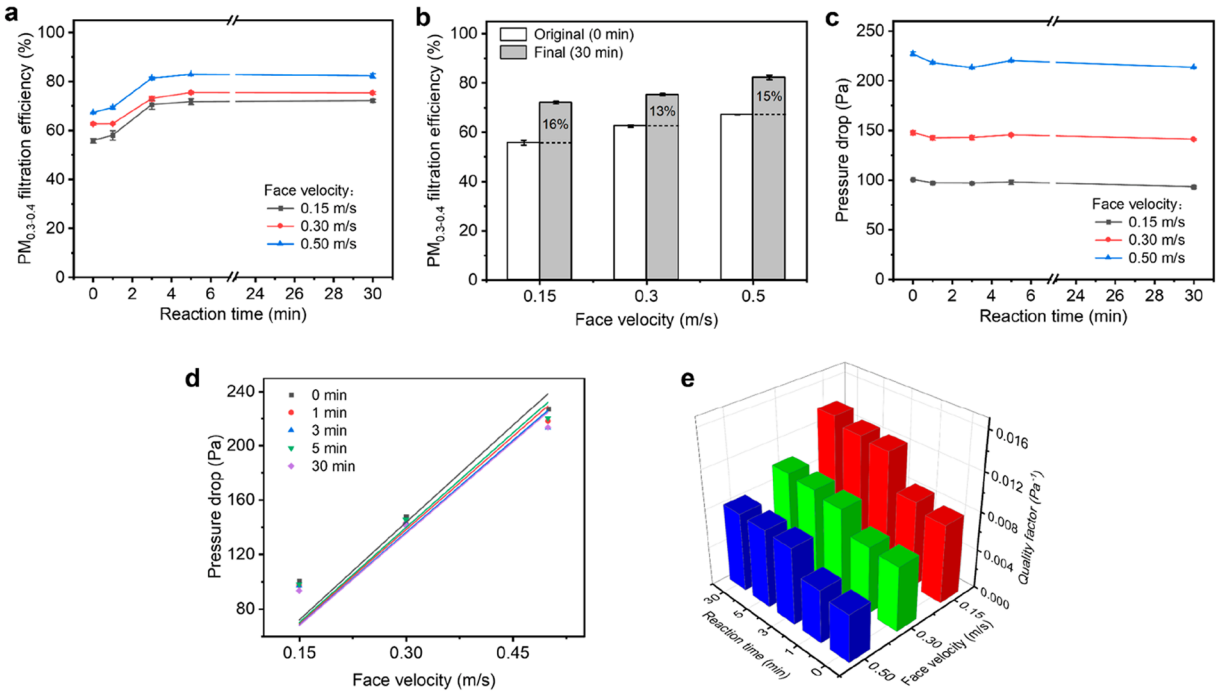

Figure 4. (a) $PM_{0.3-0.4}$ filtration efficiency vs reaction time, (b) comparison between original and final $PM_{0.3-0.4}$ filtration efficiency, (c) pressure drop vs reaction time, (d) linear regression of pressure drop, and (e) quality factor of PAN/ZIF-67 hybrid nanofiber filters under different face velocities (t_s = 1.5 h).

2.3. Measurements of Particle Filtration Performance. The particle filtration efficiency and pressure drop of the PAN/ZIF-67 hybrid nanofiber filters were tested with the use of an experimental setup as shown in Figure 2. First, compressed air was purified by a clean air supplier (3074B, TSI Inc.) and then injected into an atomizer (3076, TSI Inc.) to generate sodium chloride particles (NaCl, GR, 99.8%, Aladdin, China). The air with the NaCl particles was then dried by a diffusion dryer filled with silica gel particles (3062, TSI Inc.) and discharged by an X-ray aerosol neutralizer (3088, TSI Inc.). Finally, the particle concentration in the airflow was diluted to 1/100 by an aerosol diluter (3332, TSI Inc.), and this air was used as the particle source. An adjustable-speed fan was used to supply airflow with the desired face velocity, and the air was filtered by a commercial HEPA filter to remove background particles. The size-dependent particle concentrations were measured by two particle counters (9306, TSI Inc.). For determination of the pressure drop across the fabricated filters, the particle counters were exchanged for a manometer (621, TPI Inc.). The face velocity was measured by an air velocity meter (9545, TSI USA) and controlled at 0.15, 0.3, and 0.5 m/s, respectively. The particle filtration efficiency, η, can be calculated by

$$\eta = \frac{C_{in} - C_{out}}{C_{in}} \times 100\% \quad (1)$$

where C_{in} and C_{out} are the particle concentration upstream and downstream of the filter, respectively. The quality factor (Q_f, Pa^{-1}) of the filter can be calculated by

$$Q_f = \frac{-\ln(1 - \eta)}{\Delta P} \quad (2)$$

2.4. Characterizations. The surface morphology of the prepared filters was investigated by a scanning electron microscopy (SEM, JSM-7800F, JEOL). The crystalline structures were determined from the X-ray diffraction pattern (XRD, SmartLab) in the 2θ range from 5 to 30° with a Cu−K α radiation source. Thermogravimetric analysis (TGA) was performed with a simultaneous thermal analyzer (STA 6000, PerkinElmer) in the atmosphere of nitrogen from 30 to 500 °C with a heating rate of 10 °C/min. The change in chemical groups during the in situ growth of ZIF-67 was analyzed with a Fourier-transform infrared (FTIR) spectrometer (Alpha, Bruker).

3. RESULTS

3.1. Characterizations of PAN/ZIF-67 Hybrid Nanofiber Filters. Figure 3 presents the characterization results for PAN/ZIF-67 hybrid nanofiber filters with different reaction times. The SEM images in Figure 3a reveal a gradual increase in the growth of ZIF-67 crystals on the surface of the PAN nanofibers as the reaction time increases. The PAN nanofibers were obviously covered by ZIF-67 crystals after 5 min of reaction. However, the ZIF-67s on the surface of nanofibers did not increase significantly after 30 min of reaction, when compared to those after 5 min of reaction. That was because, the surface area of nanofibers for the growth of ZIF-67 was limited. Once the nanofibers were fully covered, it was harder to grow additional ZIF-67 crystals. As shown in the top right corner of the photographic images, the color of the filters became darker as the reaction time increased, which further demonstrates that more ZIF-67 crystals were successfully loaded on the filters. As shown in Figure 3b, the diffraction peaks of ZIF-67 (e.g., (011), (002), (112) crystal planes) gradually appeared during the reaction, which confirms the successful incorporation of ZIF-67.[40] In addition, the diffraction peaks of ZIF-67 became sharper as the reaction time increased, which also confirms the loading of increased amounts of ZIF-67. The changes in chemical groups in the electrospun nanofiber filter after the reaction were observed by FITR spectroscopy, as shown in Figure 3c. The absorption bands at 2240 cm^{-1} represent the stretching vibration of C≡N groups in PAN.[42] These bands appeared at all the different reaction times, which indicates that the PAN nanofibers were not decomposed during the ZIF-67 synthesis process. The bands observed at 1550 cm^{-1} represent the vibration of the acetate groups in metal acetate,[43] which gradually decreased as

https://doi.org/10.1021/acsami.2c06808
ACS Appl. Mater. Interfaces 2022, 14, 27096−27106

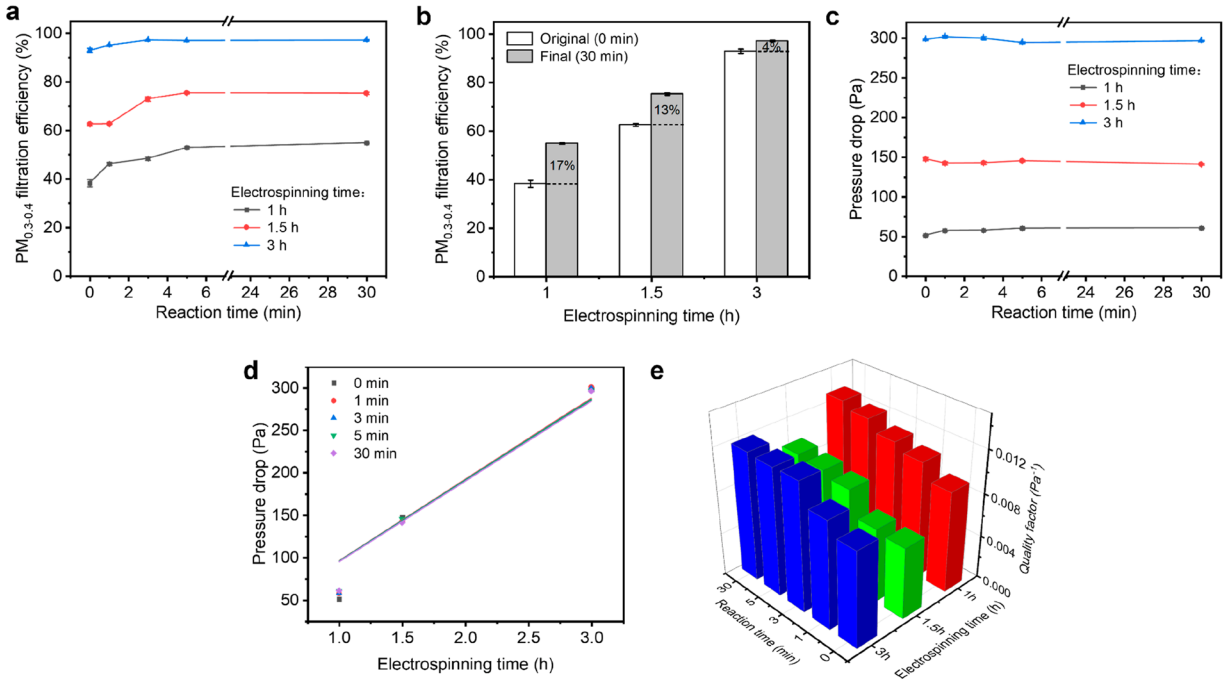

Figure 5. (a) $PM_{0.3-0.4}$ filtration efficiency vs reaction time, (b) comparison between original and final $PM_{0.3-0.4}$ filtration efficiency, (c) pressure drop vs reaction time, (d) linear regression of pressure drop, and (e) quality factor of PAN/ZIF-67 hybrid nanofiber filters with different electrospinning times (U_0 = 0.3 m/s).

the reaction time increased because the Co^{2+} was coordinated with 2-MI. The peak appearing at around 752 cm^{-1} represents the out-of-plane bending of imidazole, which indicates the successful incorporation of ZIF-67 crystals.[44] Furthermore, the N−H stretching vibration at 1846 cm^{-1} was not observed in the FTIR spectroscopy of the PAN/ZIF-67 hybrid nanofiber filters, which confirms the deprotonation of the N−H groups upon coordination with Co^{2+} ions.[40] TGA analysis was conducted to explore the thermal decomposition process of the filters with different ZIF-67 loading. As presented in Figure 3d, the PAN/ZIF-67 hybrid nanofiber filters with more ZIF-67 loading exhibited slower decomposition during the heating process. Significantly, for the filters with reaction times longer than 3 min, the weight of the filter dropped rapidly at ∼280 °C and then remained stable up to 350 °C. This occurred because ZIF-67 is thermally stable up to ∼350 °C, whereas PAN is stable only up to ∼280 °C.[45,46] Therefore, the incorporation of ZIF-67 delayed the thermal decomposition of the filters. The PAN/ZIF-67 hybrid nanofiber filters decomposed fully at 487.7 °C, which was obviously higher than the temperature for the original PAN precursor nanofiber filters (346.8 °C). This difference further indicates the successful incorporation of ZIF-67. During the in situ growth, the cobalt acetate in the PAN nanofibers dissolved into the 2-methylimidazole/ethanol solution and reacted with 2-methylimidazole to synthesize ZIF-67 on the surface of nanofibers. Namely, the loss of cobalt acetate from the nanofibers and the addition of ZIF-67 onto the nanofibers occurred simultaneously. Therefore, similar to the previous studies,[31,37,39] the real mass loading of ZIF-67 could not be measured in this study. Interestingly, the residual of the PAN/ZIF-67 filters decreased with the reaction time as shown in the TGA curves. It might be attributed to the potential reaction between PAN and ZIF-67 under the high temperature. Furthermore, as shown in Figure 3e, after bending for 20 times, the PAN/ZIF-67 hybrid nanofiber filters remained intact without cracks. Moreover, after used under a strong wind (10 m/s) for 1 h, the filters also remained intact and the ZIF-67 did not fall off from the nanofibers, as illustrated in Figure 3f. Therefore, the PAN/ZIF-67 hybrid nanofiber filers exhibited excellent flexibility and mechanical stability.

3.2. Optimal ZIF-67 Loading for Maximum Particle Filtration Performance. *3.2.1. Influence of ZIF-67 Loading under Different Face Velocities.* Figure 4 presents the influence of ZIF-67 loading on the $PM_{0.3-0.4}$ filtration performance of PAN/ZIF-67 hybrid nanofiber filters under different face velocities, when the electrospinning time was set as 1.5 h. To keep the initial structure and composition of all the filters the same, we used the PAN nanofiber filters containing cobalt acetate as the control group. As shown in Figure 4a, the $PM_{0.3-0.4}$ filtration efficiency increased with the reaction time up to 5 min. This was because the larger numbers of open metal sites and unbalanced ions of ZIF-67 increased the electrostatic effect to capture the particles. The $PM_{0.3-0.4}$ filtration efficiency then remained stable as the reaction time increased from 5 to 30 min (<1% difference). This indicates that the main ZIF-67 coordination process occurred in the first 5 min. After that, further loading of ZIF-67 was negligible, which is consistent with the characterization results in Section 3.1. Similar trends in the relationship between $PM_{0.3-0.4}$ filtration efficiency and reaction time can be observed under different face velocities, which indicates that the role of ZIF-67 in $PM_{0.3-0.4}$ capture was not influenced by the airflow rate. As shown in Figure 4b, the enhancement of $PM_{0.3-0.4}$ filtration efficiency after 30 min of reaction was greater than 13% under various face velocities. Although the original filtration efficiency increased with the face velocity, the enhancement attributed to the incorporated ZIF-67 was not apparently associated with face velocity. The pressure drop across the PAN/ZIF-67 hybrid nanofiber filters with different

https://doi.org/10.1021/acsami.2c06808
ACS Appl. Mater. Interfaces 2022, 14, 27096−27106

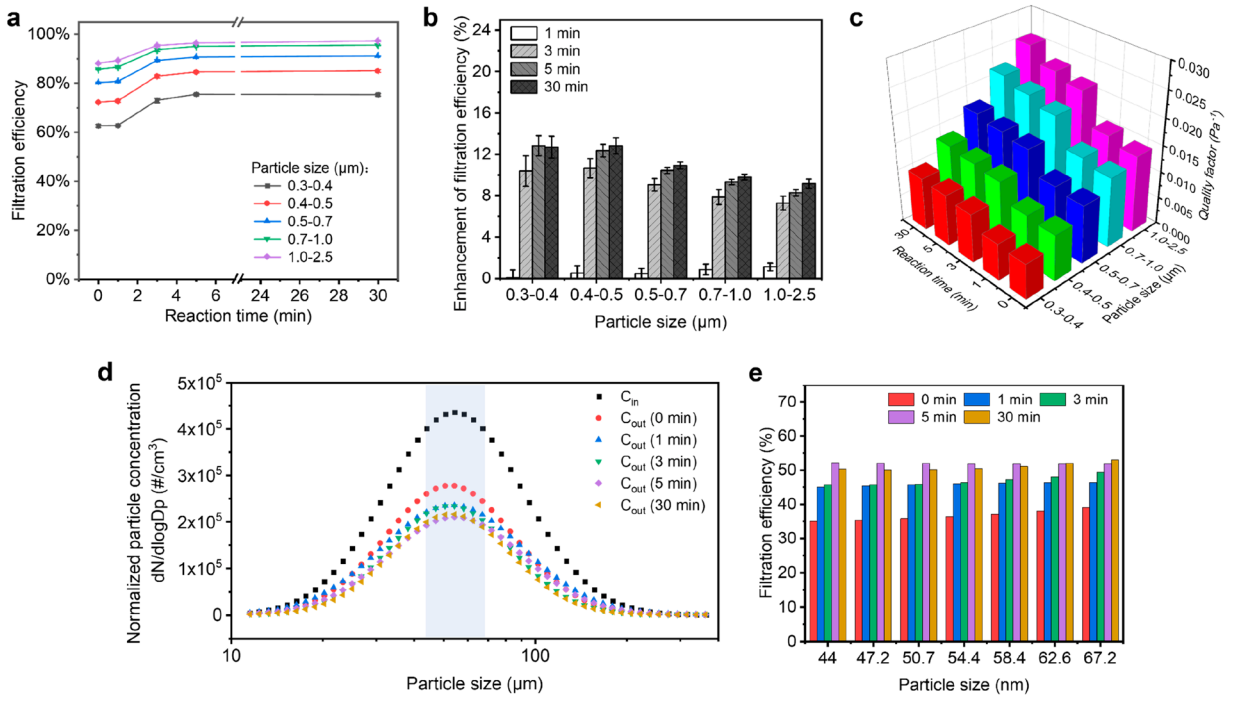

Figure 6. Size-dependent analysis of PAN/ZIF-67 hybrid nanofiber filters (U_0 = 0.3 m/s, and t_s = 1.5 h): (a) particle filtration efficiency vs reaction time, (b) enhancement of particle filtration efficiency, (c) and quality factor. Ultrafine particle filtration analysis: (d) normalized particle concentration of the original upstream flow and the flow downstream from the PAN/ZIF-67 hybrid nanofiber filters with different reaction times, and (e) the particle filtration efficiency in the selected range (44.0−67.2 nm).

reaction times is illustrated in Figure 4c. The results show that, even as more ZIF-67 crystals were loaded on the surface of the PAN nanofiber, the overall pressure drop across the nanofiber filter did not differ significantly from that across the original filters. Furthermore, as presented in Figure 4d, the pressure drop was linearly correlated with face velocity irrespective of the ZIF-67 loading amount (R^2 > 0.98 with Y-interception set at zero). The linear relationship between pressure drop and face velocity for the PAN/ZIF-67 hybrid nanofiber filters was consistent with that for pure polymer nanofiber filters.[47,48] Figure 4e displays the quality factors of PAN/ZIF-67 hybrid nanofiber filters with different reaction times under different face velocities. The quality factors increased not only with reaction time but also with face velocity. However, there was also an upper limit to the quality factor enhancement attributed to the reaction time. In summary, for the PAN/ZIF-67 hybrid nanofiber filters under different tested face velocities, a reaction time of only 5 min was sufficient for synthesis of the amount of ZIF-67 that maximized the $PM_{0.3-0.4}$ filtration efficiency. Also, the enhancement of $PM_{0.3-0.4}$ filtration efficiency was independent of face velocity, which means that PAN/ZIF-67 hybrid nanofiber filters can be used in various scenarios. With this understanding, the fabrication of PAN/ZIF-67 hybrid nanofiber filters will be more efficient in the future.

3.2.2. Influence of ZIF-67 Loading for Different Filter Thicknesses. Figure 5 illustrates the influence of ZIF-67 loading on the $PM_{0.3-0.4}$ filtration performance of PAN/ZIF-67 hybrid nanofiber filters with different electrospinning times (i.e., filter thicknesses), when the face velocity was set at 0.3 m/s. As shown in Figure 5a, the $PM_{0.3-0.4}$ filtration efficiency of the filters with different thicknesses increased with the reaction time when the time was below 5 min, and then remained stable for reaction times up to 30 min. The results also indicate that the coordination of ZIF-67 crystals to the surface of the PAN nanofibers occurred mainly in the first 5 min, which was consistent with the results presented in Section 3.2.1. However, the enhancement of $PM_{0.3-0.4}$ filtration efficiency attributed to ZIF-67 was influenced by the filter thickness. As shown in Figure 5b, the enhancement during the 30 min of reaction decreased significantly with the increase in filter thickness, from 17 to 4%. This was because, when the filter was thick enough, the particles would have been effectively captured by the filter structure, and the role of ZIF-67 was less important. The pressure drop across the PAN/ZIF-67 hybrid nanofiber filters with different reaction times is presented in Figure 5c. For the thin filter with an electrospinning time of 1 h, the pressure drop increased by 18% after 30 min of reaction, which can be attributed to the coordination of ZIF-67.[33,37] However, the filters with electrospinning times of 1.5 and 3 h exhibited a similar pressure drop (<5% difference). This indicates that the pressure drop across thicker filters was less sensitive to coordination of ZIF-67. As shown in Figure 5d, the pressure drop across PAN/ZIF-67 hybrid nanofiber filters was also linearly correlated with the electrospinning time (R^2 > 0.97 with the *Y*-intercept set at zero). According to Figure 5e, the quality factor of filters of different thicknesses also increased with the reaction time. In summary, for the PAN/ZIF-67 hybrid nanofiber filters with different thicknesses, a reaction time of only 5 min was sufficient for synthesis of the amount of ZIF-67 that maximized the $PM_{0.3-0.4}$ filtration efficiency. Meanwhile, the integration of ZIF-67 into thick filters with high original $PM_{0.3-0.4}$ filtration efficiency (>90%) was found to be unnecessary because the enhancement of filtration efficiency would not be significant.

https://doi.org/10.1021/acsami.2c06808
ACS Appl. Mater. Interfaces 2022, 14, 27096−27106

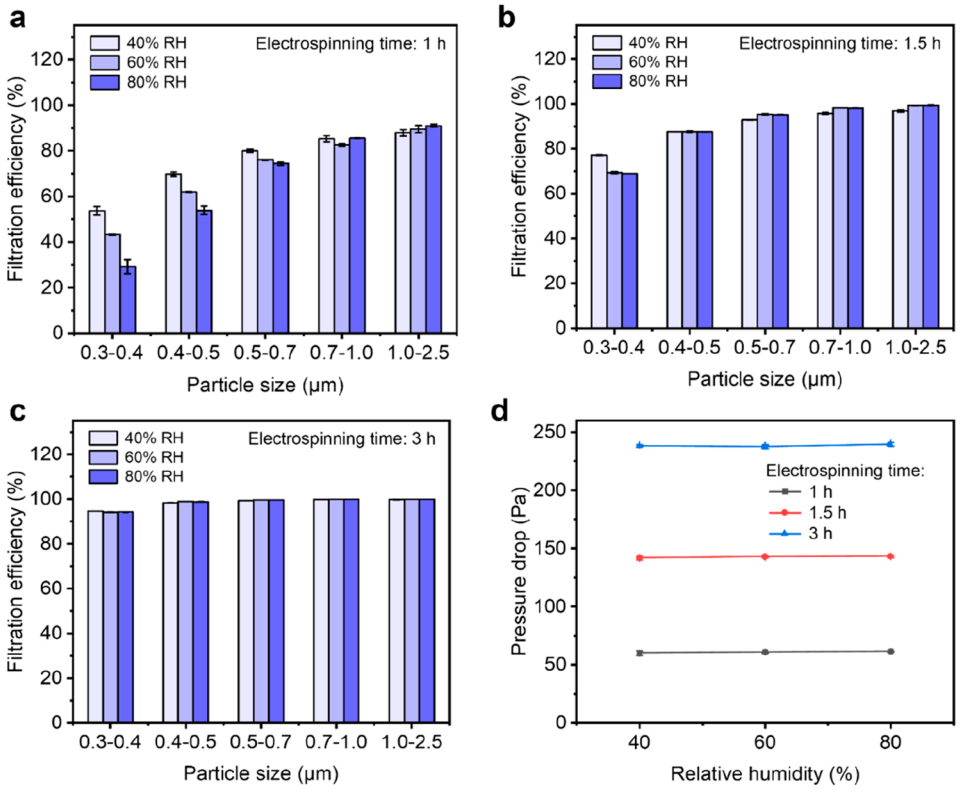

Figure 7. Particle filtration efficiency of the PAN/ZIF-67 hybrid nanofiber filters (reacted for 30 min) in different humidity conditions (40% RH, 60% RH, and 80% RH), with the electrospinning time of (a) 1, (b) 1.5, and (c) 3 h. (d) Pressure drop of the PAN/ZIF-67 hybrid nanofiber filters in different humidity conditions.

3.2.3. Influence of ZIF-67 Loading for Different Particle Sizes. Figure 6 presents the size-dependent particle filtration performance of PAN/ZIF-67 hybrid nanofiber filters with different reaction times, when the face velocity was 0.3 m/s and the electrospinning time was 1.5 h. As shown in Figure 6a, the filtration efficiency of the filters increased with particle size. This was because the increase in particle size enhanced the effects of interception and initial impaction when the particle size was greater than 0.3 μm.[15,41,49,50] Furthermore, the particle filtration efficiency increased with reaction time irrespective of particle size, which indicates that the loaded ZIF-67 contributed to the capture of particles with different sizes. The enhancement of the size-dependent particle filtration efficiency of PAN/ZIF-67 hybrid nanofiber filters with different reaction times is shown in Figure 6b. In general, the enhancement of filtration efficiency gradually decreased with the increase in particle size, e.g., from 13% (0.3−0.4 μm) to 9% (1.0−2.5 μm) for filters that reacted for 30 min. This indicates that the ZIF-67 crystals loaded on the surface of the nanofiber play a more important role in capturing smaller particles than in capturing larger particles. Figure 6c compares the particle-size-dependent quality factor of PAN/ZIF-67 hybrid nanofiber filters with different reaction times. It can be seen that the quality factor increased with both reaction time and particle size. The quality factor of PAN/ZIF-67 hybrid nanofiber filters with the most ZIF-67 loading (i.e., after a reaction time of 30 min) increased by 1.5 and 1.8 times for particle sizes of 0.3−0.4 μm and 1.0−2.5 μm, respectively, when compared with the original pure PAN nanofiber filters. The filtration efficiency of PAN/ZIF-67 hybrid nanofiber filters for ultrafine particles is presented in panels d and e in Figure 6. As shown in Figure 6d, the normalized particle concentrations in the flow downstream from the filters were significantly lower than that in the upstream flow, which indicates the effective removal of ultrafine particles. In addition, there was a greater reduction in particle concentration as the reaction time increased (i.e., with more loaded ZIF-67). To further evaluate the effects of the reaction time, we calculated the particle filtration efficiency in the particle size range from 44.0 to 67.2 nm, as the concentrations in this range were the highest. As shown in Figure 6e, the particle filtration efficiency increased with the reaction time, e.g., from 36 to 50% for a particle size of 54.4 nm. This finding demonstrates that the ZIF-67 also played a vital role in capturing ultrafine particles. In summary, for PAN/ZIF-67 hybrid nanofiber filters with an electrospinning time of 1.5 h, a reaction time of only 5 min is sufficient for synthesis of the amount of ZIF-67 that maximizes the filtration efficiency, regardless of particle size.

3.3. Influence of Humidity on Particle Filtration of PAN/ZIF-67 Filters. Figure 7 presents the size-dependent particle filtration efficiency of PAN/ZIF-67 hybrid nanofiber filters (reacted for 30 min) in different humidity conditions, when the face velocity was 0.3 m/s. As shown in Figure 7a, the filtration efficiency of particles with small sizes (0.3−0.4 μm) exhibited a noticeable reduction with the increase in relative humidity, from 54% (40% RH) to 30% (80% RH). This result indicated that the high humidity weakened the performance of PAN/ZIF-67 filters, mainly by impairing the electrostatic interaction between the particles and the nanofibers.[51] However, the influence of relative humidity gradually diminished with the increase in particle size. This phenomenon proved that the electrostatic effects played a more critical role

https://doi.org/10.1021/acsami.2c06808
ACS Appl. Mater. Interfaces 2022, 14, 27096−27106

in capturing small particles.[52] Furthermore, with the increase in filter thickness, the influence of relative humidity became negligible (as shown in Figure 7b, c), especially for the PAN/ZIF-67 filters with an electrospinning time of 3 h. This was because when the filters became thicker, the other mechanisms (e.g., interception, inertial impaction, diffusion) gradually dominated the particle filtration process.[51] In addition, the pressure drop of all PAN/ZIF-67 hybrid nanofiber filters showed negligible changes with the increase in humidity (Figure 7d). In summary, the negative effect of high humidity on the particle filtration efficiency of PAN/ZIF-67 hybrid nanofiber filters should be considered in practical applications, especially for thin filters used for capturing small particles.

4. DISCUSSION

Compared with the pure PAN nanofiber filters, the PAN/ZIF-67 hybrid nanofiber filters exhibit higher particle filtration efficiency[37] because of the enhanced electrostatic interactions.[33,36] However, the PAN/ZIF-67 hybrid nanofiber filters require additional rare materials and MOF synthesis procedures. On the basis of the findings in this study, the MOF synthesis time can be shortened from over 10 h as reported in the literature to only 5 min. Furthermore, our previous study showed that the particle filtration efficiency of PAN/ZIF-67 hybrid nanofiber filters was stable for a month with a negligible drop (<1%).[37] In addition, our previous study also showed that, after five washing cycles by ethanol, the filters can still maintain a high particle filtration efficiency.[2] Although the particle filtration efficiency cannot be directly compared with that of the other MOF-based nanofiber filters reported in the literature[2,22,37,53−57] because of the differences in particle composition and size distribution, face velocity, and testing environment, this study demonstrated that the target particle filtration efficiency can be obtained by tuning the electrospinning time and MOF loading.

There are some limitations in this study, such as the method for controlling the in situ growth of ZIF-67. As shown in Figure 5a, although the particle filtration efficiency of PAN/ZIF-67 hybrid nanofiber filters with different thicknesses reached the upper limit at around 5 min, the reaction speeds in the first 5 min were different. This indicates that, when the original filters have different filter morphologies (e.g., filter thickness, fiber diameter, packing density), the ZIF-67 loading speed may be different. In addition, the ZIF synthesis speed will be influenced by the solvents and reaction temperature,[58] the concentrations of reagents,[45] the additives used,[59] etc. Consequently, the correlation between the reaction time and the amount of loaded ZIF-67 that influences the particle filtration efficiency, may not be applicable to other in situ growth processes for MOFs. However, for electrospun polymer nanofiber filters that incorporate MOFs for particle filtration, the proposed evaluation methods in this study can be used to identify the upper limit of enhanced filtration efficiency and the corresponding reaction time. Therefore, the method for shortening the reaction process for the sake of reaching the maximum filtration performance has great potential for application in large-scale industrial production. In addition, the basic filtration mechanisms attributed to ZIF-67 still need more analysis. ZIF-67 is formed through the coordination of Co^{2+} and imidazole.[41] As a result of charge separation, Co becomes electropositive and N, in the imidazole, becomes electronegative.[36] Therefore, the electrostatic interactions generated by ZIF-67 will be beneficial for PM removal. The ZIF-67 also enhanced the surface roughness of the filters when compared to the original PAN nanofibers, which were smooth (as illustrated in Figure 3). The cross-sectional shape of the nanofibers was modified by the loaded ZIF-67 crystals, and the projected area was increased,[60] in contrast with the circular cross-section of the original PAN nanofibers. Namely, more stagnation regions were created by the modified boundary layer because of the protuberances.[61,62] However, the increase in surface roughness by MOFs has not been clearly explored in the existing studies. Consequently, in the present study we proposed that the enhancement of particle filtration efficiency was also partially caused by elevated surface roughness attributed to the ZIF-67 crystals. In future work, we will investigate the influence of surface roughness separately and evaluate its contribution to the enhancement of particle filtration efficiency.

5. CONCLUSIONS

In this study, different amounts of ZIF-67 crystals were grown in situ on electrospun PAN nanofiber filters through control of the reaction time. The characterization results demonstrated that ZIF-67 was successfully coordinated to the PAN nanofiber filters at different reaction times. Next, the particle filtration efficiency of PAN/ZIF-67 hybrid nanofiber filters under different face velocities and with different filter thicknesses was measured and analyzed. Finally, the filtration performance of PAN/ZIF-67 hybrid nanofiber filters for ultrafine particles was investigated. Within the scope of this research, the following conclusions can be drawn:

1. The surface morphology and chemical composition changed with the amount of ZIF-67 loading on the PAN/ZIF-67 hybrid nanofiber filters.
2. For filters with different thicknesses, a reaction time of only 5 min was sufficient for synthesis of the amount of ZIF-67 that maximized the $PM_{0.3-0.4}$ filtration efficiency.
3. The enhancement of $PM_{0.3-0.4}$ filtration efficiency attributed to ZIF-67 was independent of face velocity, which means that the PAN/ZIF-67 hybrid nanofiber filters can be utilized in various application scenarios.
4. It is not necessary to integrate ZIF-67 into thick filters with high original $PM_{0.3-0.4}$ filtration efficiency (>90%), because the enhancement in filtration efficiency would not be significant.
5. The enhancement of filtration efficiency for ultrafine particles was positively correlated with the amount of ZIF-67 incorporated into the PAN/ZIF-67 hybrid nanofiber filters.
6. This study shortened the synthesis time of the in situ incorporation of MOFs into electrospun nanofiber filters from more than 10 h (reported in the literature) to only 5 min.

AUTHOR INFORMATION

Corresponding Author

Chun Chen − *Department of Mechanical and Automation Engineering, The Chinese University of Hong Kong, Shatin N.T. 999077 Hong Kong SAR, China; Shenzhen Research Institute, The Chinese University of Hong Kong, Shenzhen 518057, China*; Email: chunchen@mae.cuhk.edu.hk

https://doi.org/10.1021/acsami.2c06808
ACS Appl. Mater. Interfaces 2022, 14, 27096−27106

Authors

Zhuolun Niu − *Department of Mechanical and Automation Engineering, The Chinese University of Hong Kong, Shatin N.T. 999077 Hong Kong SAR, China;* orcid.org/0000-0003-4596-712X

Can Xiao − *Department of Mechanical and Automation Engineering, The Chinese University of Hong Kong, Shatin N.T. 999077 Hong Kong SAR, China*

Jinhan Mo − *Department of Building Science, Tsinghua University, Beijing 100084, China;* orcid.org/0000-0002-3178-6507

Li Zhang − *Department of Mechanical and Automation Engineering, The Chinese University of Hong Kong, Shatin N.T. 999077 Hong Kong SAR, China;* orcid.org/0000-0003-1152-8962

Complete contact information is available at: https://pubs.acs.org/10.1021/acsami.2c06808

Notes

The authors declare no competing financial interest.

■ ACKNOWLEDGMENTS

This work was partially supported by the General Research Fund of Research Grants Council of Hong Kong SAR, China (Grant 14204520) and the Hong Kong Centre for Logistics Robotics.

■ REFERENCES

(1) Air Pollution. World Health Organization. https://www.who.int/health-topics/air-pollution (accessed 2022-02-23).

(2) Bian, Y.; Chen, C.; Wang, R.; Wang, S.; Pan, Y.; Zhao, B.; Chen, C.; Zhang, L. Effective Removal of Particles down to 15 nm Using Scalable Metal-Organic Framework-Based Nanofiber Filters. *Appl. Mater. Today* **2020**, *20*, 100653.

(3) Kim, K. H.; Kabir, E.; Kabir, S. A Review on the Human Health Impact of Airborne Particulate Matter. *Environ. Int.* **2015**, *74*, 136−143.

(4) Apte, J. S.; Brauer, M.; Cohen, A. J.; Ezzati, M.; Pope, C. A. Ambient PM2.5 Reduces Global and Regional Life Expectancy. *Environ. Sci. Technol. Lett.* **2018**, *5* (9), 546−551.

(5) Balakrishnan, K.; Dey, S.; Gupta, T.; Dhaliwal, R. S.; Brauer, M.; Cohen, A. J.; Stanaway, J. D.; Beig, G.; Joshi, T. K.; Aggarwal, A. N.; Sabde, Y.; Sadhu, H.; Frostad, J.; Causey, K.; Godwin, W.; Shukla, D. K.; Kumar, G. A.; Varghese, C. M.; Muraleedharan, P.; Agrawal, A.; Anjana, R. M.; Bhansali, A.; Bhardwaj, D.; Burkart, K.; Cercy, K.; Chakma, J. K.; Chowdhury, S.; Christopher, D. J.; Dutta, E.; Furtado, M.; Ghosh, S.; Ghoshal, A. G.; Glenn, S. D.; Guleria, R.; Gupta, R.; Jeemon, P.; Kant, R.; Kant, S.; Kaur, T.; Koul, P. A.; Krish, V.; Krishna, B.; Larson, S. L.; Madhipatla, K.; Mahesh, P. A.; Mohan, V.; Mukhopadhyay, S.; Mutreja, P.; Naik, N.; Nair, S.; Nguyen, G.; Odell, C. M.; Pandian, J. D.; Prabhakaran, D.; Prabhakaran, P.; Roy, A.; Salvi, S.; Sambandam, S.; Saraf, D.; Sharma, M.; Shrivastava, A.; Singh, V.; Tandon, N.; Thomas, N. J.; Torre, A.; Xavier, D.; Yadav, G.; Singh, S.; Shekhar, C.; Vos, T.; Dandona, R.; Reddy, K. S.; Lim, S. S.; Murray, C. J. L.; Venkatesh, S.; Dandona, L. The Impact of Air Pollution on Deaths, Disease Burden, and Life Expectancy across the States of India: The Global Burden of Disease Study 2017. *Lancet Planet. Heal.* **2019**, *3* (1), e26−e39.

(6) Ohlwein, S.; Kappeler, R.; Kutlar Joss, M.; Künzli, N.; Hoffmann, B. Health Effects of Ultrafine Particles: A Systematic Literature Review Update of Epidemiological Evidence. *Int. J. Public Health* **2019**, *64* (4), 547−559.

(7) Elder, A.; Gelein, R.; Silva, V.; Feikert, T.; Opanashuk, L.; Carter, J.; Potter, R.; Maynard, A.; Ito, Y.; Finkelstein, J.; Oberdörster, G. Translocation of Inhaled Ultrafine Manganese Oxide Particles to the Central Nervous System. *Environ. Health Perspect.* **2006**, *114* (8), 1172−1178.

(8) Liu, Y.; Ning, Z.; Chen, Y.; Guo, M.; Liu, Y.; Gali, N. K.; Sun, L.; Duan, Y.; Cai, J.; Westerdahl, D.; et al. Aerodynamic Analysis of SARS-CoV-2 in Two Wuhan Hospitals. *Nature* **2020**, *582* (7813), 557−560.

(9) Chen, C.; Zhao, B. Review of Relationship between Indoor and Outdoor Particles: I/O Ratio, Infiltration Factor and Penetration Factor. *Atmos. Environ.* **2011**, *45* (2), 275−288.

(10) Lee, K. W.; Liu, B. Y. H. Theoretical Study of Aerosol Filtration by Fibrous Filters. *Aerosol Sci. Technol.* **1982**, *1* (2), 147−161.

(11) Liu, H.; Cao, C.; Huang, J.; Chen, Z.; Chen, G.; Lai, Y. Progress on Particulate Matter Filtration Technology: Basic Concepts, Advanced Materials, and Performances. *Nanoscale* **2020**, *12* (2), 437−453.

(12) Chen, C.; Zhao, B. Review of Relationship between Indoor and Outdoor Particles: I/O Ratio, Infiltration Factor and Penetration Factor. *Atmos. Environ.* **2011**, *45* (2), 275−288.

(13) Fazli, T.; Zeng, Y.; Stephens, B. Fine and Ultrafine Particle Removal Efficiency of New Residential HVAC Filters. *Indoor Air* **2019**, *29* (4), 656−669.

(14) Montgomery, J. F.; Green, S. I.; Rogak, S. N.; Bartlett, K. Predicting the Energy Use and Operation Cost of HVAC Air Filters. *Energy Build.* **2012**, *47*, 643−650.

(15) Ben-David, T.; Waring, M. S. Interplay of Ventilation and Filtration: Differential Analysis of Cost Function Combining Energy Use and Indoor Exposure to PM2.5 and Ozone. *Build. Environ.* **2018**, *128*, 320−335.

(16) Xiang, J.; Huang, C. H.; Austin, E.; Shirai, J.; Liu, Y.; Seto, E. Energy Consumption of Using HEPA-Based Portable Air Cleaner in Residences: A Monitoring Study in Seattle, US. *Energy Build.* **2021**, *236*, 110773.

(17) Xue, J.; Xie, J.; Liu, W.; Xia, Y. Electrospun Nanofibers: New Concepts, Materials, and Applications. *Acc. Chem. Res.* **2017**, *50* (8), 1976−1987.

(18) Xue, J.; Wu, T.; Dai, Y.; Xia, Y. Electrospinning and Electrospun Nanofibers: Methods, Materials, and Applications. *Chem. Rev.* **2019**, *119* (8), 5298−5415.

(19) Zhao, X.; Wang, S.; Yin, X.; Yu, J.; Ding, B. Slip-Effect Functional Air Filter for Efficient Purification of PM 2.5. *Sci. Rep.* **2016**, *6*, 35472.

(20) Zhu, M.; Han, J.; Wang, F.; Shao, W.; Xiong, R.; Zhang, Q.; Pan, H.; Yang, Y.; Samal, S. K.; Zhang, F.; Huang, C. Electrospun Nanofibers Membranes for Effective Air Filtration. *Macromol. Mater. Eng.* **2017**, *302* (1), 1600353.

(21) Zhang, S.; Rind, N. A.; Tang, N.; Liu, H.; Yin, X.; Yu, J.; Ding, B. *Electrospun Nanofibers for Air Filtration*; Elsevier, 2018.

(22) Gao, Y.; Tian, E.; Zhang, Y.; Mo, J. Utilizing Electrostatic Effect in Fibrous Filters for Efficient Airborne Particles Removal: Principles, Fabrication, and Material Properties. *Appl. Mater. Today* **2022**, *26*, 101369.

(23) Peterson, G. W.; Lee, D. T.; Barton, H. F.; Epps, T. H.; Parsons, G. N. Fibre-Based Composites from the Integration of Metal-Organic Frameworks and Polymers. *Nat. Rev. Mater.* **2021**, *6* (7), 605−621.

(24) Kim, Y.; Wu, X.; Lee, C.; Oh, J. H. Characterization of PI/PVDF-TrFE Composite Nanofiber-Based Triboelectric Nanogenerators Depending on the Type of the Electrospinning System. *ACS Appl. Mater. Interfaces* **2021**, *13* (31), 36967.

(25) Zhu, M.; Hua, D.; Pan, H.; Wang, F.; Manshian, B.; Soenen, S. J.; Xiong, R.; Huang, C. Green Electrospun and Crosslinked Poly(Vinyl Alcohol)/Poly(Acrylic Acid) Composite Membranes for Antibacterial Effective Air Filtration. *J. Colloid Interface Sci.* **2018**, *511*, 411−423.

(26) Almasian, A.; Olya, M. E.; Mahmoodi, N. M. Preparation and Adsorption Behavior of Diethylenetriamine/Polyacrylonitrile Composite Nanofibers for a Direct Dye Removal. *Fibers Polym.* **2015**, *16* (9), 1925−1934.

(27) Dou, Y.; Zhang, W.; Kaiser, A. Electrospinning of Metal-Organic Frameworks for Energy and Environmental Applications. *Adv. Sci.* **2020**, *7* (3), 1902590.
(28) Oveisi, M.; Alinia Asli, M.; Mahmoodi, N. M. Carbon Nanotube Based Metal-Organic Framework Nanocomposites: Synthesis and Their Photocatalytic Activity for Decolorization of Colored Wastewater. *Inorg. Chim. Acta* **2019**, *487*, 169−176.
(29) Mahmoodi, N. M.; Oveisi, M.; Bakhtiari, M.; Hayati, B.; Shekarchi, A. A.; Bagheri, A.; Rahimi, S. Environmentally Friendly Ultrasound-Assisted Synthesis of Magnetic Zeolitic Imidazolate Framework - Graphene Oxide Nanocomposites and Pollutant Removal from Water. *J. Mol. Liq.* **2019**, *282*, 115−130.
(30) Zhang, Y.; Yuan, S.; Feng, X.; Li, H.; Zhou, J.; Wang, B. Preparation of Nanofibrous Metal-Organic Framework Filters for Efficient Air Pollution Control. *J. Am. Chem. Soc.* **2016**, *138* (18), 5785−5788.
(31) Zhao, J.; Lee, D. T.; Yaga, R. W.; Hall, M. G.; Barton, H. F.; Woodward, I. R.; Oldham, C. J.; Walls, H. J.; Peterson, G. W.; Parsons, G. N. Ultra-Fast Degradation of Chemical Warfare Agents Using MOF-Nanofiber Kebabs. *Angew. Chemie - Int. Ed.* **2016**, *55* (42), 13224−13228.
(32) Lee, D. T.; Zhao, J.; Peterson, G. W.; Parsons, G. N. Catalytic "MOF-Cloth" Formed via Directed Supramolecular Assembly of UiO-66-NH2 Crystals on Atomic Layer Deposition-Coated Textiles for Rapid Degradation of Chemical Warfare Agent Simulants. *Chem. Mater.* **2017**, *29* (11), 4894−4903.
(33) Zhang, Y.; Yuan, S.; Feng, X.; Li, H.; Zhou, J.; Wang, B. Preparation of Nanofibrous Metal-Organic Framework Filters for Efficient Air Pollution Control. *J. Am. Chem. Soc.* **2016**, *138* (18), 5785−5788.
(34) Huang, R. J.; Zhang, Y.; Bozzetti, C.; Ho, K. F.; Cao, J. J.; Han, Y.; Daellenbach, K. R.; Slowik, J. G.; Platt, S. M.; Canonaco, F.; et al. High Secondary Aerosol Contribution to Particulate Pollution during Haze Events in China. *Nature* **2014**, *514* (7521), 218−222.
(35) Zhang, R.; Liu, C.; Hsu, P. C.; Zhang, C.; Liu, N.; Zhang, J.; Lee, H. R.; Lu, Y.; Qiu, Y.; Chu, S.; Cui, Y. Nanofiber Air Filters with High-Temperature Stability for Efficient PM2.5 Removal from the Pollution Sources. *Nano Lett.* **2016**, *16* (6), 3642−3649.
(36) Yoo, D. K.; Woo, H. C.; Jhung, S. H. Removal of Particulate Matters by Using Zeolitic Imidazolate Framework-8s (ZIF-8s) Coated onto Cotton: Effect of the Pore Size of ZIF-8s on Removal. *ACS Appl. Mater. Interfaces* **2021**, *13* (29), 35214−35222.
(37) Bian, Y.; Wang, R.; Wang, S.; Yao, C.; Ren, W.; Chen, C.; Zhang, L. Metal-Organic Framework-Based Nanofiber Filters for Effective Indoor Air Quality Control. *J. Mater. Chem. A* **2018**, *6* (32), 15807−15814.
(38) Liang, H.; Jiao, X.; Li, C.; Chen, D. Flexible Self-Supported Metal-Organic Framework Mats with Exceptionally High Porosity for Enhanced Separation and Catalysis. *J. Mater. Chem. A* **2018**, *6* (2), 334−341.
(39) Wang, C.; Cheng, P.; Yao, Y.; Yamauchi, Y.; Yan, X.; Li, J.; Na, J. In-Situ Fabrication of Nanoarchitectured MOF Filter for Water Purification. *J. Hazard. Mater.* **2020**, *392*, 122164.
(40) Zhou, K.; Mousavi, B.; Luo, Z.; Phatanasri, S.; Chaemchuen, S.; Verpoort, F. Characterization and Properties of Zn/Co Zeolitic Imidazolate Frameworks vs. ZIF-8 and ZIF-67. *J. Mater. Chem. A* **2017**, *5* (3), 952−957.
(41) Hu, M.; Yin, L.; Low, N.; Ji, D.; Liu, Y.; Yao, J.; Zhong, Z.; Xing, W. Zeolitic-Imidazolate-Framework Filled Hierarchical Porous Nanofiber Membrane for Air Cleaning. *J. Membr. Sci.* **2020**, *594*, 117467.
(42) Li, W.; Yang, Z.; Zhang, G.; Meng, Q. Heat-Treated Polyacrylonitrile (PAN) Hollow Fiber Structured Packings in Isopropanol (IPA)/Water Distillation with Improved Thermal and Chemical Stability. *Ind. Eng. Chem. Res.* **2013**, *52* (19), 6492−6501.
(43) Nickolov, Z.; Georgiev, G.; Stoilova, D.; Ivanov, I. Raman and IR Study of Cobalt Acetate Dihydrate. *J. Mol. Struct.* **1995**, *354* (2), 119−125.
(44) Li, Z.; Zhou, G.; Dai, H.; Yang, M.; Fu, Y.; Ying, Y.; Li, Y. Biomineralization-Mimetic Preparation of Hybrid Membranes with Ultra-High Loading of Pristine Metal-Organic Frameworks Grown on Silk Nanofibers for Hazard Collection in Water. *J. Mater. Chem. A* **2018**, *6* (8), 3402−3413.
(45) Qian, J.; Sun, F.; Qin, L. Hydrothermal Synthesis of Zeolitic Imidazolate Framework-67 (ZIF-67) Nanocrystals. *Mater. Lett.* **2012**, *82* (2012), 220−223.
(46) Zhang, W. X.; Wang, Y. Z.; Sun, C. F. Characterization on Oxidative Stabilization of Polyacrylonitrile Nanofibers Prepared by Electrospinning. *J. Polym. Res.* **2007**, *14* (6), 467−474.
(47) Xia, T.; Bian, Y.; Zhang, L.; Chen, C. Relationship between Pressure Drop and Face Velocity for Electrospun Nanofiber Filters. *Energy Build.* **2018**, *158*, 987−999.
(48) Bian, Y.; Zhang, L.; Chen, C. Experimental and Modeling Study of Pressure Drop across Electrospun Nanofiber Air Filters. *Build. Environ.* **2018**, *142* (June), 244−251.
(49) Lee, K. W.; Liu, B. Y. H. On the Minimum Efficiency and the Most Penetrating Particle Size for Fibrous Filters. *J. Air Pollut. Control Assoc.* **1980**, *30* (4), 377−381.
(50) Liu, H.; Zhang, S.; Liu, L.; Yu, J.; Ding, B. High-Performance PM0.3 Air Filters Using Self-Polarized Electret Nanofiber/Nets. *Adv. Funct. Mater.* **2020**, *30* (13), 1909554.
(51) Zhou, C.; Han, W.; Yang, X.; Fan, H.; Li, C.; Dong, L.; Meng, H. Electrospun Polyetherimide/Zeolitic Imidazolate Framework Nanofibrous Membranes for Enhanced Air Filtration Performance under High Temperature and High Humidity Conditions. *Chem. Eng. J.* **2022**, *433* (P3), 134069.
(52) Bai, Y.; Han, C. B.; He, C.; Gu, G. Q.; Nie, J. H.; Shao, J. J.; Xiao, T. X.; Deng, C. R.; Wang, Z. L. Washable Multilayer Triboelectric Air Filter for Efficient Particulate Matter PM2.5 Removal. *Adv. Funct. Mater.* **2018**, *28* (15), 1706680.
(53) Chen, Y.; Zhang, S.; Cao, S.; Li, S.; Chen, F.; Yuan, S.; Xu, C.; Zhou, J.; Feng, X.; Ma, X.; Wang, B. Roll-to-Roll Production of Metal-Organic Framework Coatings for Particulate Matter Removal. *Adv. Mater.* **2017**, *29* (15), 1606221.
(54) Feng, S.; Li, X.; Zhao, S.; Hu, Y.; Zhong, Z.; Xing, W.; Wang, H. Multifunctional Metal Organic Framework and Carbon Nanotube-Modified Filter for Combined Ultrafine Dust Capture and SO2 Dynamic Adsorption. *Environ. Sci. Nano* **2018**, *5* (12), 3023−3031.
(55) Hu, M.; Yin, L.; Low, N.; Ji, D.; Liu, Y.; Yao, J.; Zhong, Z.; Xing, W. Zeolitic-Imidazolate-Framework Filled Hierarchical Porous Nanofiber Membrane for Air Cleaning. *J. Membr. Sci.* **2020**, *594*, 117467.
(56) Ma, S.; Zhang, M.; Nie, J.; Tan, J.; Yang, B.; Song, S. Design of Double-Component Metal-Organic Framework Air Filters with PM2.5 Capture, Gas Adsorption and Antibacterial Capacities. *Carbohydr. Polym.* **2019**, *203*, 415−422.
(57) Yoo, D. K.; Woo, H. C.; Jhung, S. H. Removal of Particulate Matters with Isostructural Zr-Based Metal-Organic Frameworks Coated on Cotton: Effect of Porosity of Coated MOFs on Removal. *ACS Appl. Mater. Interfaces* **2020**, *12* (30), 34423−34431.
(58) Lee, Y. R.; Jang, M. S.; Cho, H. Y.; Kwon, H. J.; Kim, S.; Ahn, W. S. ZIF-8: A Comparison of Synthesis Methods. *Chem. Eng. J.* **2015**, *271*, 276.
(59) Cravillon, J.; Nayuk, R.; Springer, S.; Feldhoff, A.; Huber, K.; Wiebcke, M. Controlling Zeolitic Imidazolate Framework Nano- and Microcrystal Formation: Insight into Crystal Growth by Time-Resolved in Situ Static Light Scattering. *Chem. Mater.* **2011**, *23* (8), 2130−2141.
(60) Wang, N.; Si, Y.; Wang, N.; Sun, G.; El-Newehy, M.; Al-Deyab, S. S.; Ding, B. Multilevel Structured Polyacrylonitrile/Silica Nanofibrous Membranes for High-Performance Air Filtration. *Sep. Purif. Technol.* **2014**, *126*, 44−51.
(61) Hosseini, S. A.; Tafreshi, H. V. On the Importance of Fibers' Cross-Sectional Shape for Air Filters Operating in the Slip Flow Regime. *Powder Technol.* **2011**, *212* (3), 425−431.

https://doi.org/10.1021/acsami.2c06808
ACS Appl. Mater. Interfaces 2022, 14, 27096−27106

(62) Hosseini, S. A.; Tafreshi, H. V. Modeling Particle Filtration in Disordered 2-D Domains: A Comparison with Cell Models. *Sep. Purif. Technol.* **2010**, *74* (2), 160−169.

https://doi.org/10.1021/acsami.2c06808
ACS Appl. Mater. Interfaces 2022, 14, 27096−27106